Applied Catalysis B: Environmental 180 (2016) 121–129

Contents lists available at ScienceDirect

Applied Catalysis B: Environmental

journal homepage: www.elsevier.com/locate/apcatb

Carbon dispersed copper-cobalt alloy nanoparticles: A cost-effective heterogeneous catalyst with exceptional performance in the hydrolytic dehydrogenation of ammonia-borane

Ahmet Bulut[a], Mehmet Yurderi[a], İlknur Efecan Ertas[a], Metin Celebi[a], Murat Kaya[b], Mehmet Zahmakiran[a,*]

[a] Department of Chemistry, Science Faculty, Yüzüncü Yıl University, 65080 Van, Turkey
[b] Department of Chemical Engineering and Applied Chemistry, Atilim University, 06836 Ankara, Turkey

ARTICLE INFO

Article history:
Received 29 March 2015
Received in revised form 5 June 2015
Accepted 11 June 2015
Available online 17 June 2015

Keywords:
Ammonia-Borane
Hydrogen storage
Copper
Cobalt
Alloy
Nanoparticles

ABSTRACT

Herein, we report the development of a new and cost-effective nanocatalyst for the hydrolytic dehydrogenation of ammonia-borane (NH_3BH_3), which is considered to be one of the most promising solid hydrogen carriers due to its high gravimetric hydrogen storage capacity (19.6 wt%) and low molecular weight. The new catalyst system consisting of bimetallic copper-cobalt alloy nanoparticles supported on activated carbon was simply and reproducibly prepared by surfactant-free deposition-reduction technique at room temperature. The characterization of this new catalytic material was done by the combination of multi-pronged techniques including ICP-MS, XRD, XPS, BFTEM, HR-TEM, STEM and HAADF-STEM-line analysis. The sum of their results revealed that the formation of copper-cobalt alloy nanoparticles (d_{mean} = 1.8 nm) on the surface of activated carbon (CuCo/C). These new carbon supported copper-cobalt alloy nanoparticles act as highly active catalyst in the hydrolytic dehydrogenation of ammonia-borane, providing an *initial* turnover frequency of TOF = 2700 h^{-1} at 298 K, which is not only higher than all the non-noble metal catalysts but also higher than the majority of the noble metal based homogeneous and heterogeneous catalysts employed in the same reaction. More importantly, easy recovery and high durability of these supported CuCo nanoparticles make CuCo/C recyclable heterogeneous catalyst for the hydrolytic dehydrogenation of ammonia-borane. They retain almost their inherent activity even at 10th catalytic reuse in the hydrolytic dehydrogenation of ammonia-borane at 298 K.

1. Introduction

Hydrogen has been considered as a promising and clean energy carrier [1,2] for our future society as it has a high energy density (142 MJ/kg) almost three times higher than that of natural gas (55 MJ/kg) and only water plus small amounts of heat are the byproducts when it is utilized in proton exchange membrane fuel cells (PEMFC) [3,4]. Although there has been enormous efforts to develop suitable hydrogen storage and releasing materials in the last few decades, the efficient storage and production of hydrogen are still two key problems in the "Hydrogen Economy" [5]. Among the new hydrogen storage materials [6,7], ammonia-borane (H_3NBH_3, AB) appears to be the most promising material for this purpose [8] because of its low molecular weight (30.9 g/mol), high stability under possible fuel cell applications, nontoxicity, and high hydrogen density (19.6 wt%), which is greater than the 2015 target of U.S. Department of Energy (5.5 wt% H_2) [9]. To date thermal decomposition [10], alcoholysis [11] or dehydrocoupling [12] have been demonstrated to provoke the hydrogen release from AB. Although, difficulties in the regeneration of hydrolysis products due to the strong B—O bonds, there is much interest in the transition-metal-catalyzed hydrolytic dehydrogenation of AB (**1**) due to favorable kinetics and mild reaction conditions [13].

$$H_3NBH_3 + 2H_2O \rightarrow NH_4BO_2 + 3H_2 \quad (1)$$

The literature survey shows that various homogeneous [8] and heterogeneous [13–16] catalysts have already been tested in the hydrolytic dehydrogenation of AB. Although, some of homogeneous catalysts provide high activities and selectivities in the

* Corresponding author. Fax: +90 432 225 18 06.
E-mail address: zmehmet@yyu.edu.tr (M. Zahmakiran).
URL: http://www.nanomatcat.com (M. Zahmakiran).

http://dx.doi.org/10.1016/j.apcatb.2015.06.021
0926-3373/

hydrolytic dehydrogenation of AB, the difficulties met during their isolation-recovery steps hinder their practical application for onboard systems. At this concern, because of the advantages of nanocatalysis [17], the current research has been concentrated on the development of metal nanoparticles (NPs) possessing high activity and reusability in the hydrolytic dehydrogenation of AB. Among tested heterogeneous catalysts precious metals (such as Rh [18–21], Pt [18,19] and Au [22–24]) based systems provide remarkable activities in the hydrolytic dehydrogenation of AB. However, the concerns over the practical use of these high cost metals have motivated the research for the development of low cost catalyst systems in the hydrolytic dehydrogenation of AB. In this context, the recent studies have revealed that heterogeneous catalysts of low-cost 3d metals such as Fe [25–27], Co [28–37], Ni [38–44] and Cu [45–48] can catalyze the hydrolytic dehydrogenation of AB. Unfortunately, most of these low-cost catalytic systems suffer from low activity and reusability performance. Hereof, the development of highly active and reusable heterogeneous catalysts based on low-cost 3d metals is clearly a desired goal for this important reaction.

In this study, we report a facile synthesis of bimetallic copper-cobalt alloy NPs supported on activated carbon, hereafter referred to as CuCo/C, and their excellent catalysis in the hydrolytic dehydrogenation of AB. CuCo/C catalyst was simply and reproducibly prepared through surfactant-free deposition-reduction technique [49] at room temperature, and characterized by inductively coupled plasma-optical emission spectroscopy (ICP-OES), powder X-ray diffraction (PXRD), high resolution X-ray photoelectron spectroscopy (HRXPS), bright field transmission electron microscopy (BFTEM), high resolution transmission electron microscopy (HRTEM), scanning transmission electron microscopy (STEM) and high angle annular dark field-scanning transmission electron microscopy (HAADF-STEM). The sum of their results revealed that the formation of well-dispersed 1.8 ± 0.4 nm CuCo alloy NPs on the surface of activated carbon. These new CuCo alloy NPs provide exceptional activity (TOF = 2700 h^{-1}) and reusability (>95% activity and >90% conversion at 10th reuse) performance in the hydrolytic dehydrogenation of AB at room temperature. Moreover, the excellent durability of supported CuCo alloy NPs against to sintering and leaching make CuCo/C reusable catalyst for the hydrolytic dehydrogenation of AB.

2. Experimental

2.1. Materials

Copper(II) chloride dihydrate ($CuCl_2{\cdot}2H_2O$), cobalt(II) sulfate heptahydrate ($CoSO_4{\cdot}7H_2O$), ammonia-borane ($NH_3BH_3 \sim 90\%$), sodium borohydride ($NaBH_4$), boron trifluoride diethyl etherate ($BF_3{\cdot}(C_2H_5)_2O$) and activated carbon were purchased from Sigma–Aldrich®. Deionized water was distilled by water purification system (Milli-Q Water Purification System). All glassware and Teflon-coated magnetic stir bars were washed with acetone and copiously rinsed with distilled water before drying in an oven at 323 K.

2.2. Characterization

Cu and Co contents of the samples were determined by ICP-OES (Leeman, Direct Reading Echelle) after each sample was completely dissolved in a mixture of HNO_3/HCl (1/3 ratio). PXRD patterns were recorded with a MAC Science MXP 3TZ diffractometer using Cu-Kα radiation (wavelength 1.54 Å, 40 kV, 55 mA). BFTEM, HRTEM, STEM, and HAADF-STEM samples were pre-pared by dropping one drop of dilute suspension on copper coated carbon TEM grid and the solvent was then dried. BFTEM was carried out on a JEOL JEM-200CX transmission electron microscopes operating at 120 kV. HRTEM, STEM, and HAADF-STEM were run on a JEOL JEM-2010F transmission electron microscope operating at 200 kV. Oxford EDXS system and Inca software were used to collect and process STEM-EDX data. HRXPS analyses were performed on a Physical Electronics 5800 spectrometer equipped with a hemispherical analyzer and using monochromatic Al-Kα radiation (1486.6 eV, the X-ray tube working at 15 kV and 350 W, and pass energy of 23.5 eV). ^{11}B NMR spectra were recorded on a Bruker Avance DPX 400 with an operating frequency of 128.15 MHz. D_2O and $BF_3{\cdot}(C_2H_5)_2O$ were used as a lock and an external reference, respectively. At the end of the catalytic reaction, the resulting solutions were filtered and the filtrates were collected for taking the ^{11}B NMR spectra.

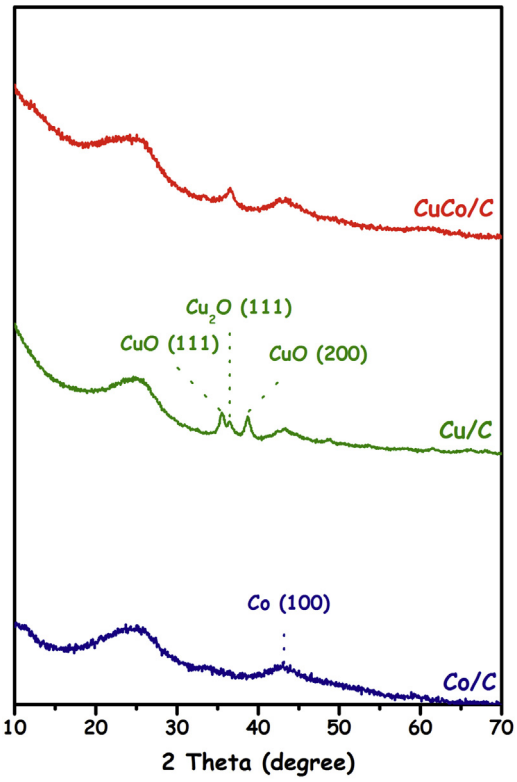

Fig. 1. The powder X-ray diffraction (P-XRD) patterns of Co/C, Cu/C and CuCo/C samples in the range of $2\theta = 10–70^{\circ}$.

2.3. Preparation of CuCo/C catalyst

In a typical experiment, 5.0 mL of aqueous solution containing 24.0 μmol copper (4,09 mg $CuCl_2.2H_2O$) and 24.2 μmol cobalt (6,8 mg $CoSO_4.7H_2O$) is mixed with activated carbon (140 mg) at 400 rpm for 2 h. Then, 1.0 mL aqueous solution of $NaBH_4$ (27.8 mg, 0.60 mmol) was added to this mixture and the resulting solution was stirred for half an hour under air at room temperature. After centrifugation (6000 rpm, 5 min.), copious washing with water (3×20 mL), filtration, and drying in vacuum oven at 323 K under 10^{-2} Torr, CuCo/C catalyst was obtained as powder and stored under argon atmosphere in the glovebox.

2.4. Determination of the catalytic activity of CuCo/C Catalyst in the hydrolytic dehydrogenation of ammonia-borane

The catalytic activity of CuCo/C catalyst in the hydrolytic dehydrogenation of AB was determined by measuring the rate of hydrogen generation. The volume of released gas during the reac-

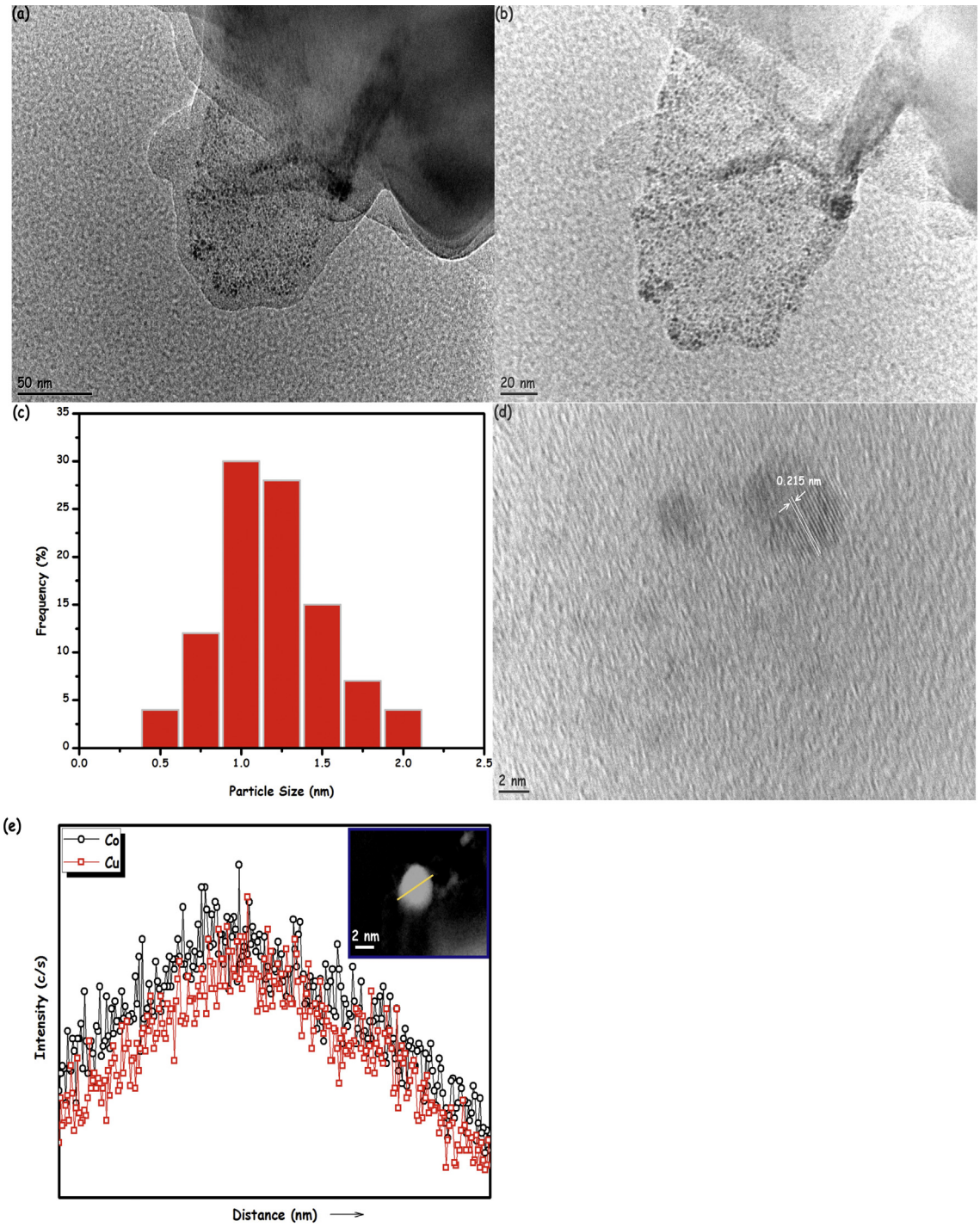

Fig. 2. (a) and (b) BFTEM images of CuCo/C at different magnifications and corresponding size histogram (*inset* (b)), (c) HRTEM image of CuCo/C and (d) HAADF-STEM line-scan analyses using STEM-EDX for Cu and Co along the yellow arrow given in HAADF-STEM image (*inset*).

tion was monitored using the gas burette by water displacement. Before starting the catalytic activity test, a jacketed one necked reaction flask (50.0 mL) containing a Teflon-coated stir bar was placed on a magnetic stirrer (Heidolph MR-3004) and thermostated to 298 K by using a constant temperature bath (Lab Companion RW-0525). In a typical experiment, CuCo/C catalyst was weighed and transferred into the reaction flask and then 4.0 mL H_2O was added into the reaction flask under argon purging and this mixture was stirred for 15 min. to achieve thermal equilibrium. Next, 1.0 mL aqueous solution of AB (17.5 mg, 0.5 mmol) was added into the reaction flask via its septum by using a 1.0 mL gastight syringe and the catalytic reaction was started (t = 0 min) by stirring the mixture at 600 rpm.

2.5. Reusability performance of CuCo/C catalyst in the hydrolytic dehydrogenation of ammonia-borane

After the first run of hydrolytic dehydrogenation of aqueous AB solution (100 mM in 5.0 mL H_2O) starting with CuCo/C at 298 K, the catalyst was isolated from reaction solution by centrifugation and washed with excess water, then dried at 398 K. The dried catalyst

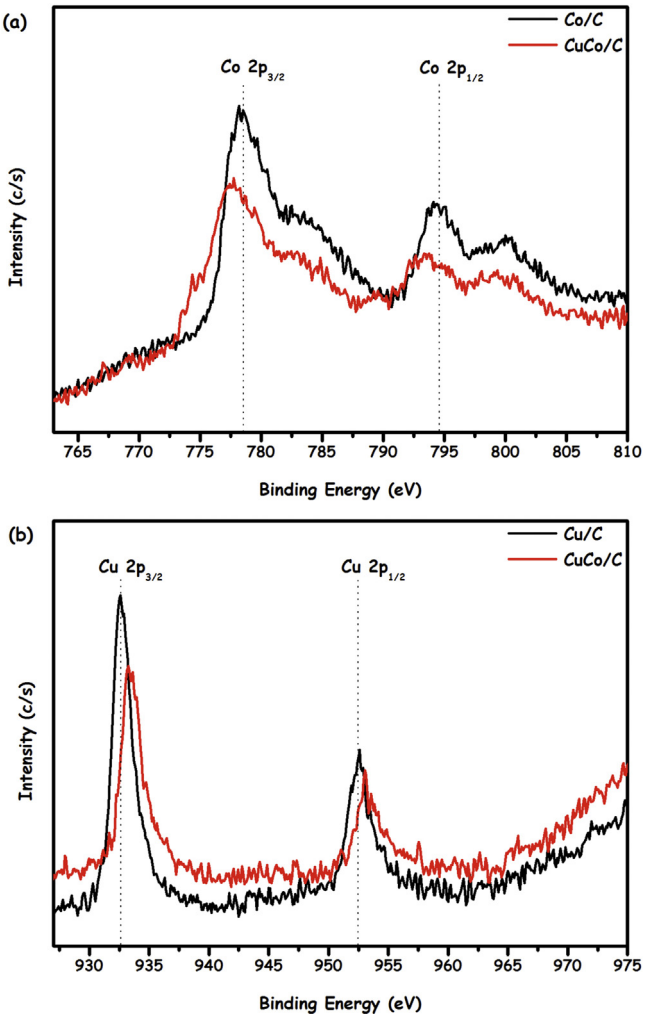

Fig. 3. The high resolution (a) Co 2p XPS spectra for Co/C and CuCo/C, (b) Cu 2p XPS spectra for Cu/C and CuCo/C samples.

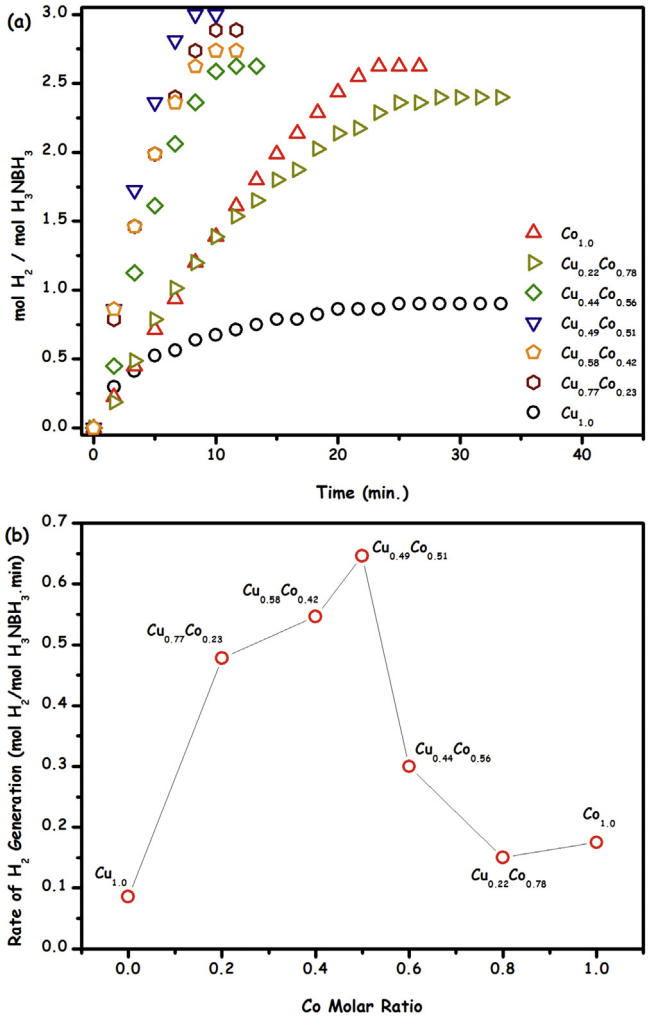

Fig. 4. (a) The plot of mol H_2/mol NH_3BH_3 versus time (min.) graph for the hydrolytic dehydrogenation of AB ([AB]/[metal] ~30) starting with different mono and bimetallic Cu-Co NPs at 298 K°C, (b) The plot of hydrogen generation rate (mol H_2/mol H_3NBH_3.min) versus Co molar ratio.

was weighted and used again in the hydrolytic dehydrogenation of aqueous AB solution (100 mM in 5.0 mL H_2O) at 298 K.

3. Results and discussion

3.1. Preparation and characterization of CuCo/C catalyst

CuCo/C catalyst was simply and reproducibly prepared by surfactant-free deposition-reduction technique [49] at room temperature. Typically, an aqueous solution containing copper(II) chloride, cobalt(II) sulfate and activated carbon was mixed to impregnate Cu^{2+} and Co^{2+} on carbon surface. Next, sodium borohydride as a reducing agent was added to this mixture and the resulting solution was stirred for half an hour under air at room temperature. After centrifugation, copious washing with water and dried in vacuum oven at 323 K under 10^{-2} Torr; CuCo/C catalyst was obtained as black powder and characterized by ICP-OES, PXRD, HRXPS, BFTEM, HR-TEM, STEM and HAADF-STEM-line analysis. The elemental composition of the as-prepared catalyst was found to be $Cu_{0.49}Co_{0.51}$/C (11.9 μmol Cu, 12.1 μmol Co corresponds to 0.53 wt% and 0.50 wt% Co loadings, respectively) by ICP-OES analyses. Fig. 1 depicts P-XRD patterns of Cu/C, Co/C and CuCo/C materials. Co/C and Cu/C samples gives diffraction peaks at 43.1°, 35.4°, 36.5° and 38.7°, which can be assigned to Co [100] (JCPDS No. 15-808), CuO [111] (JCPDS No. 48-1548), Cu_2O [111] (JCPDS No. 78-2076) and

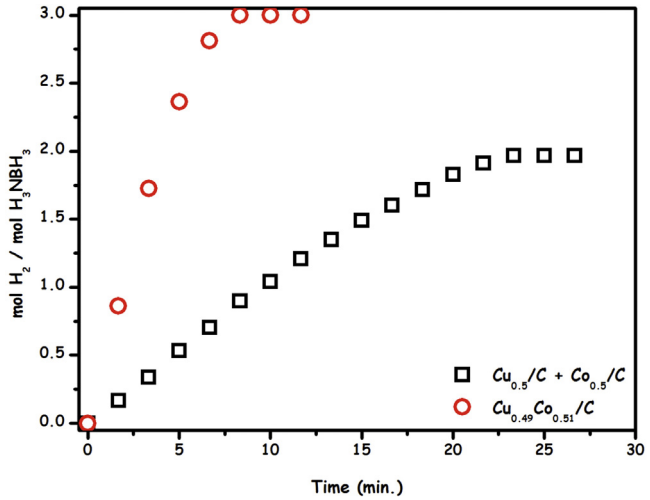

Fig. 5. The plot for mol H_2/mol NH_3BH_3 versus time (min.) corresponding to the hydrolytic dehydrogenation of AB ([AB]/[metal] ~30) at 298 K in the presence of $Cu_{0.49}Co_{0.51}$/C (○) or the physical mixture of ($Cu_{0.50}$/C + $Co_{0.50}$/C) (□).

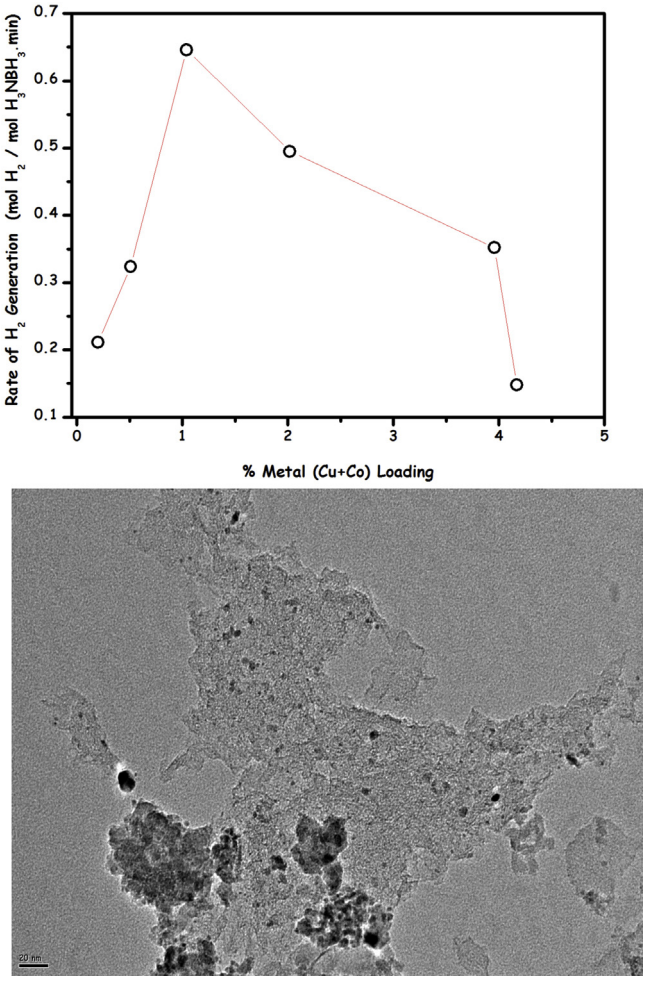

Fig. 6. The plot of hydrogen generation rate (mol H_2/mol H_3NBH_3.min) versus metal loading (wt%) for CuCo/C catalyzed hydrolytic dehydrogenation of AB ([AB]/[metal] ~30) at 298 K and BFTEM image of CuCo/C catalyst with 4.17 wt% metal (Cu + Co) loading.

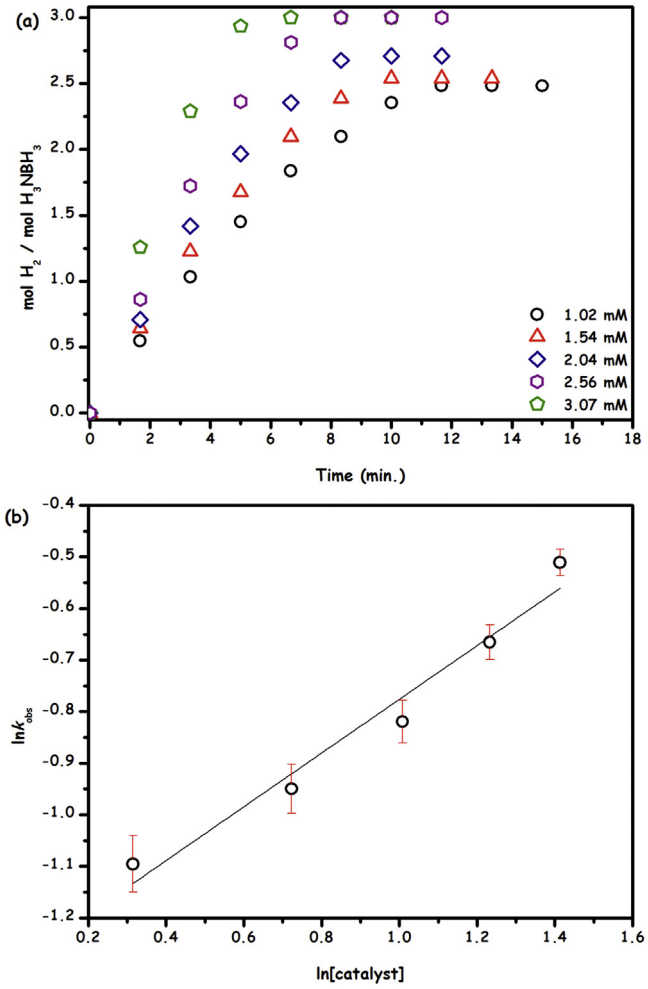

Fig. 7. (a) The plot of mol H_2 / mol NH_3BH_3 versus time (min.) graph, (b) The plot of the gas generation rate versus the catalyst concentration (both in logarithmic scale) for the hydrolytic dehydrogenation of AB ([AB] = 100 mM in 5.0 mL H_2O) starting with different $Cu_{0.49}Co_{0.51}$/C concentrations at 298 K.

CuO [200], respectively [50], whereas CuCo/C exhibits a diffraction peak in the position between Co [100] and CuO [200], whose position is also differs from Cu [111] [51]. The main reason for the observation of cuprous oxide and copper oxide phases is the high oxophilicity of copper(0), which has high tendency to form oxides under aerobic conditions [52,53].

BFTEM, HRTEM, and HAADF-STEM investigations were performed to examine the size, morphology and the composition of the $Cu_{0.49}Co_{0.51}$/C catalyst. BFTEM images of $Cu_{0.49}Co_{0.51}$/C given in Figs. 2 (a) and (b) reveal the presence of CuCo NPs. The mean particle size for the images given in Figs. 2 (a) and (b) was found to be ca. 1.8 nm using the NIH image program [54], which included the particle size analysis for > 50 non-touching particles (Fig. 2 (b) *inset*). HRTEM image of $Cu_{0.49}Co_{0.51}$/C is given in Fig. 2(c) is displaying the highly crystalline nature of the resulting CuCo NPs on the activated carbon surface. The fringe distance was measured to be 0.215 nm, which is different from Cu [111] (0.200 nm), Cu_2O [111] (0.242 nm), CuO [111] (0.205 nm), CuO [200] (0.232 nm) [55] and Co [100] (0.220 nm) [55], and can be assignable to CuCo alloy structure. Furthermore, the formation of alloy structure was also confirmed by HAADF-STEM-line analysis (Fig. 2(d)). When the distribution of Cu and Co in the randomly chosen particle was assessed by using the line scanning analysis in the STEM-EDX mode, we can clearly see the overlapping of Cu and Co signals that can be assignable to the formation of alloy structure in CuCo NPs. These results support the presence of CuCo alloy NPs on the support surface. On the other hand, as it is difficult to establish a true statistical analysis using microscopic probes, presence of a minor amount of overlapping domains of separately nucleated Cu and Co NPs cannot be excluded.

Additionally, XPS results (Fig. 3) show that the binding energies for Co 2p are shifted to lower values compared with those in Co/C, whereas the binding energies for Cu 2p in $Cu_{0.49}Co_{0.51}$/C are shifting to higher value relative to those in Cu/C. These shifts reveal that some electrons are transferred from Cu to Co in the alloy structure of $Cu_{0.49}Co_{0.51}$/C catalyst. It can be understood that Cu atoms are closely interacting with Co in the alloy structure and electrons can be transferred from Cu to Co to equilibrate the Fermi level because of the difference of work functions of $Cu_{(100)}$ (4.65 eV) [56,57] and $Co_{(100)}$ (5.44 eV) [58]. Such electron transfer in $Cu_{0.49}Co_{0.51}$/C has the potential deign itself with the high activity to H_2 generation from aqueous AB solution at room temperature (*vide infra*) [52].

3.2. CuCo/C catalyzed hydrolyticdehydrogenation of ammonia-borane

For a comprehensive elucidation of the catalytic activity of the CuCo/C catalytic architecture towards hydrolytic dehydrogenation of AB; we followed a systematic approach, where the individual catalytic performance of each structural subcomponent (*i.e.* single-component samples such as $Cu_{1.0}$/C and $Co_{1.0}$/C) was stud-

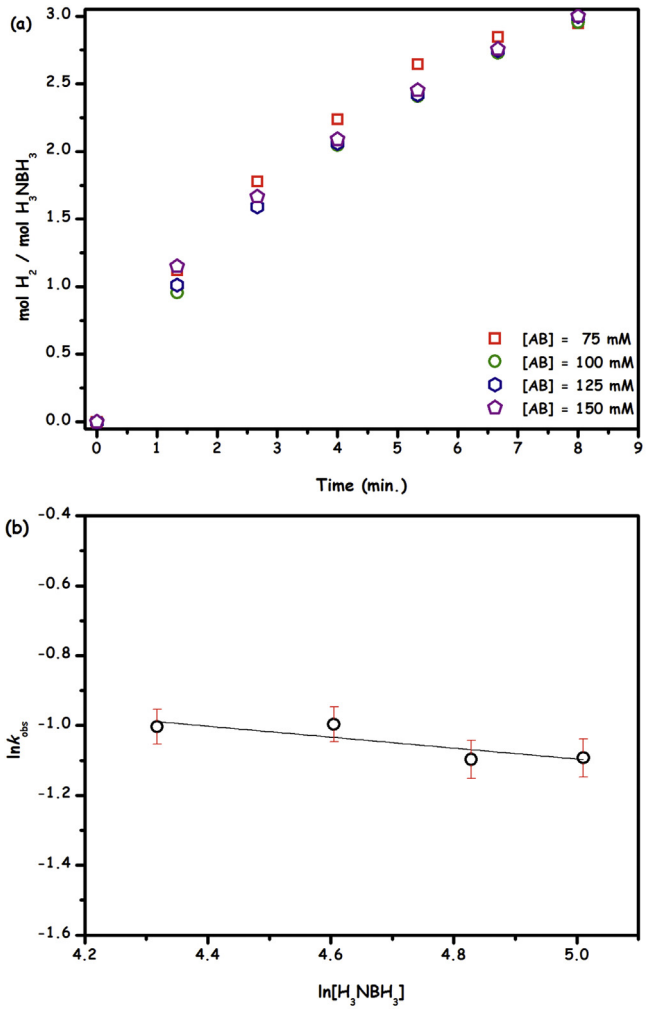

Fig. 8. (a) The plot of mol H_2 / mol NH_3BH_3 versus time (min.) graph, (b) The plot of the gas generation rate versus the AB concentration (both in logarithmic scale) for the $Cu_{0.49}Co_{0.51}$/C catalyzed ([catalyst] = 3.43 mM in 5.0 mL H_2O) hydrolytic dehydrogenation of AB starting with different AB concentrations at 298 K

ied in addition to binary combinations of these subcomponents (*i.e.* $Cu_{0.22}Co_{0.78}$/C, $Cu_{0.44}Co_{0.56}$/C, $Cu_{0.49}Co_{0.51}$/C, $Cu_{0.58}Co_{0.42}$/C, $Cu_{0.77}Co_{0.23}$/C) and their results are given in Fig. 4(a). Evidently, $Cu_{0.49}Co_{0.51}$/C catalyst provides the best activity compared to all other investigated catalysts. The observed "volcano"-type activity (Fig. 4(b)) of the CuCo/C catalyst versus Cu/Co molar composition indicates that neither Cu nor Co has enough activity for catalyzing the hydrolytic dehydrogenation of AB at complete conversion. Alloying Cu with Co provides a required synergistic effect on the catalysis and $Cu_{0.49}Co_{0.51}$ is the optimum catalyst to achieve complete hydrolytic dehydrogenation of AB. This result is also showing that Cu and Co form a uniform alloy structure in the preparation. The uniqueness of the $Cu_{0.49}Co_{0.51}$/C catalyst structure was further supported by a control experiment where a physical mixture of $Cu_{0.50}$/C and $Co_{0.50}$/C exhibited a significantly lower activity than that of $Cu_{0.49}Co_{0.51}$/C catalyst in the hydrolytic dehydrogenation of AB at 298 K (Fig. 5). This control experiment demonstrates a proximity requirement associated with the synergistic structural components of the $Cu_{0.49}Co_{0.51}$/C catalyst, which interact in an efficient manner during the hydrolytic dehydrogenation of AB.

Then, in a series of experiment the catalytic activity of CuCo/C catalyst with various metal ([Cu + Co]) loadings in the range of 0.20–4.20 wt% were tested in the hydrolytic dehydrogenation of AB at 298 K to determine the effect of metal loading on CuCo/C activity. The hydrogen generation rates were found to be 0.240, 0.324, 0.646, 0.495, 0.352 and 0.148 mol H_2/mol H_3NBH_3.min for CuCo/C catalyst containing 0.20, 0.51, 1.04, 2.05, 3.96 and 4.20% wt metal loadings, respectively (Fig. 6). The variation in catalytic activities reflects the change in the number of active sites of CuCo NPs. For example, BFTEM image of CuCo/C catalyst with 4.20% wt metal loading (Fig. 6) shows the existence of agglomerates, which can explain the lowest activity observed at 5.1% wt metal loading. For all other test reactions performed in this study, samples of CuCo/C catalyst containing ~0.77 wt% metal were used.

Fig. 7(a) shows the plots of mol H_2/mol H_3NBH_3 versus time (min.) during the hydrolytic dehydrogenation of AB in the presence of $Cu_{0.49}Co_{0.51}$/C catalyst in different metal concentrations at 298 K. As expected from preformed catalysts, a linear hydrogen generation starts without induction time period and continues until the complete consumption of AB. We found that only 3.4 mol% of $Cu_{0.49}Co_{0.51}$/C can catalyze the hydrolytic dehydrogenation of AB at complete conversion (3.0 mol H_2/mol AB corresponds to ~0.04 wt% of H_2 releasing relative to catalyst, solvent and starting ammonia-borane used in the experiment, which is lower than 2015 target of USA DOE [5]). The *initial* TOF value was found to be 1720 mol H_2 mol catalyst^{-1} h^{-1} and to the best of our knowledge this is the highest TOF value among the first row metal catalysts used in the hydrolytic dehydrogenation of AB (Table 1).

Moreover, this TOF value is also higher than that of obtained by precious metal based heterogeneous and homogeneous catalysts such as Pt (150 mol catalyst^{-1} h^{-1}) [18], PtO_2 (1125 mol catalyst^{-1} h^{-1}) [18], K_2PtCl_4 (474 mol catalyst^{-1} h^{-1}) [18], Pd (31.2 mol catalyst^{-1} h^{-1}) [18], Ru NPs (1800 mol catalyst^{-1} h^{-1}) [59], Ir NPs (170 mol catalyst^{-1} h^{-1}) [60], Rh/TiO_2 (15 mol catalyst^{-1} h^{-1}) [61], Pd/zeolite (400 mol catalyst^{-1} h^{-1}) [62], [IrHCl{$(PPh_2(o\text{-}C_6H_4CO))_2H$}] (300 mol catalyst^{-1} h^{-1}) [63], Ir-PNP complex (250 mol catalyst^{-1} h^{-1}) [64]. The reaction rates for each catalyst concentration were calculated from the linear portion of each plot. The logarithmic plot of the hydrogen generation rate versus catalyst concentration (Fig. 7(b)) gives the line with a slope of 0.52 indicative of the catalytic reaction is close to half-order with respect to the catalyst concentration.

It should be noted that, aside from the volumetric measurement of the hydrogen gas evolution, the completion of hydrolytic dehydrogenation was also ascertained by using ^{11}B-{^1H}-NMR spectroscopy. After the reaction, the signal of H_3NBH_3 at $\delta = 24.2$ ppm (q) completely disappears and a new resonance at $\delta = 9.0$ ppm (s) shows up, which is readily assigned to the metaborate (BO_2) anion. The quantity of ammonia liberated during $Cu_{0.49}Co_{0.51}$/C catalyzed hydrolytic dehydrogenation of AB was investigated by control tests using copper(II) sulfate or acid/base indicator, which showed no ammonia evolution in detectable amount in the experiments. The effect of substrate concentration on the hydrogen generation rate was also studied by performing a series of experiments starting with varying initial concentration of AB while the catalyst concentration is kept constant ([CuCo] = 3.41 mM). Fig. 8(a) shows the plots of mol H_2/mol H_3NBH_3 versus time during $Cu_{0.49}Co_{0.51}$/C catalyzed hydrolytic dehydrogenation of AB for various initial concentrations of AB at 298 K. As given in Fig. 8(b) the catalytic reaction was found to be zero-order with respect to substrate concentration at room temperature.

In addition to the effect of [catalyst] and [substrate] concentrations on the dehydrogenation rate, we also investigated the dehydrogenation rate depending on the temperature to find the activation energy (Ea), activation enthalpy ($\Delta H^{\neq}$) and activation entropy ($\Delta S^{\neq}$) values. For this purpose, $Cu_{0.49}Co_{0.51}$/C catalyzed hydrolytic dehydrogenation of AB was carried out at different temperatures in the range of 298-328 K and their results are given in Fig. 9(a), which shows the increase in hydrogen generation rate in parallel to temperature increase. The values of observed rate

Table 1
First-row-metal-based catalyst systems employed in the hydrolysis of ammonia borane at 298 K and their activity/reusability performances tabulated from scifinder literature search.

Entry	(pre) Catalyst	n_{AB}/n_{metal}	TOF[a,b]	Retained activity at reuse	Reference
1	Fe NPs	8.3	280	Nd[c]	[25]
2	Co/Al_2O_3	56	130	Nd	[28]
3	Ni/Al_2O_3	56	135	Nd	[28]
4	Fe/Al_2O_3	56	0	Nd	[28]
5	Co NPs	25	980	80% at 5th reuse	[29]
6	Co NPs	50	840	Nd	[30]
7	Co/zeolite	50	240	60% at 5th reuse	[33]
8	Co/SiO_2 nanosphere	20	760	75% at 10th reuse	[34]
9	Co/SiO_2	20	480	50% at 10th reuse	[34]
10	Co NPs	50	920	Nd	[35]
11	Ni NPs	50	600	Nd	[35]
12	$Co@SiO_2$	83	800	72% at 10th reuse	[36]
13	CuCo/MIL-101	30	1180	95 at 5th reuse	[37]
14	Ni NPs	10	234	60% at 5th reuse	[38]
15	$Ni@SiO_2$	20	212	Nd	[39]
16	Ni NPs	10	41	87% at 10th reuse	[40]
17	Ni NPs	20	530	80% at 5th reuse	[41]
18	Ni/zeolite	25	305	78% at 5th reuse	[42]
19	$Cu@Cu_2O$	25	15	Nd	[45]
20	Cu/zeolite	75	50	50% at 5th reuse	[46]
21	$Ni\text{-}SiO_2$	30	30	60% at 5th reuse	[43]
22	Cu/Co_3O_4	30	880	Nd	[47]
23	Cu@SCF	90	1020	85% at 10th reuse	[48]
24	Co-Ni-W-B	20	600	87% at 10th reuse	[43]
25	$Cu_{0.49}Co_{0.51}/C$	30	1720	95% at 10th reuse	This study

[a] TOF = mol H_2/mol metal h calculated at 20% conversion is reached; [b]These TOF values are not corrected for the number of exposed surface atoms; that is, the values given are lower limits; [c]Nd: not demonstrated.

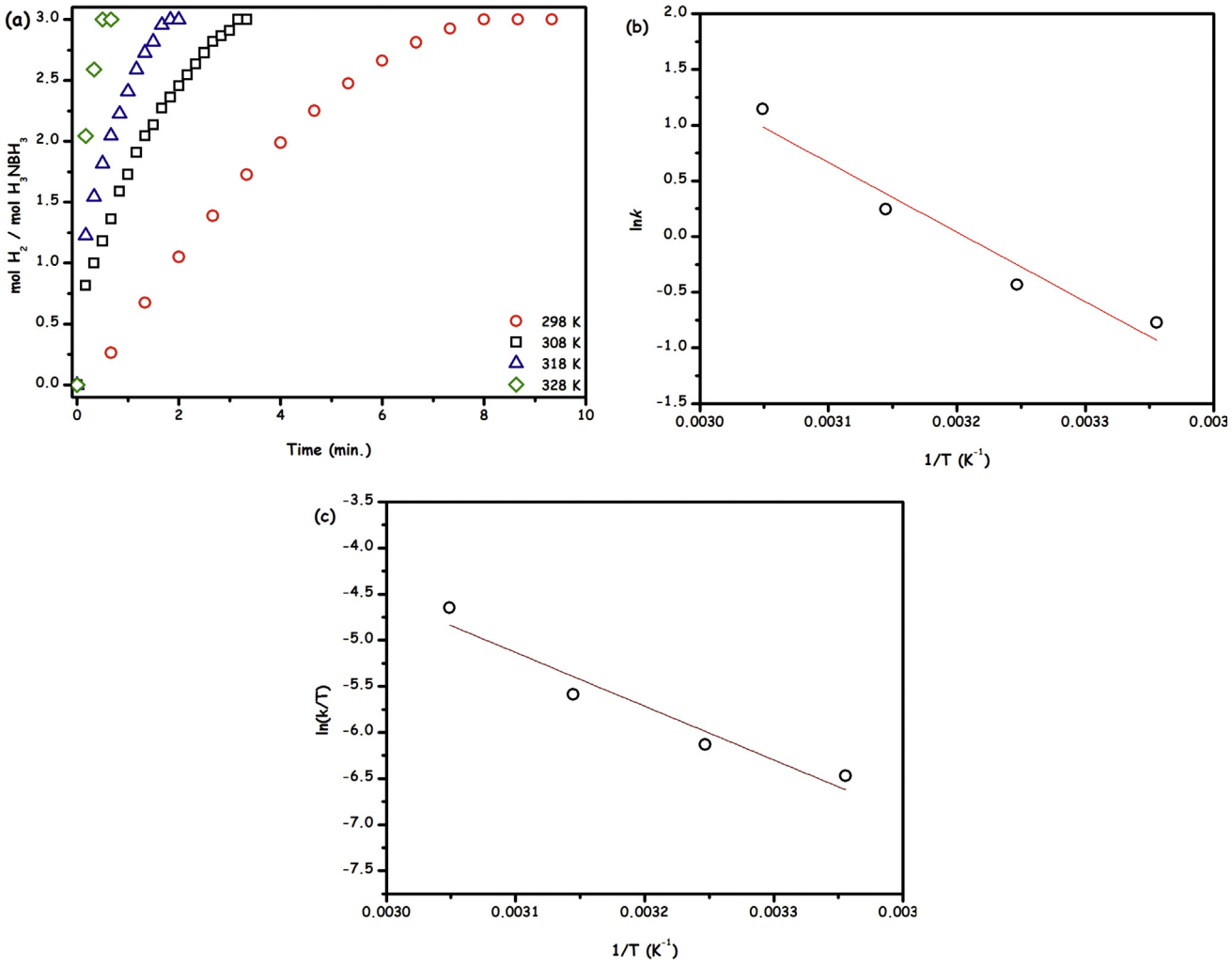

Fig. 9. (a) The plot of mol H_2/mol NH_3BH_3 versus time (min.) graph, (b) Arrhenius plot, (c) Eyring plot for the $Cu_{0.49}Co_{0.51}/C$ catalyzed hydrolytic dehydrogenation of AB ([AB]/[metal] ~30) at different temperatures.

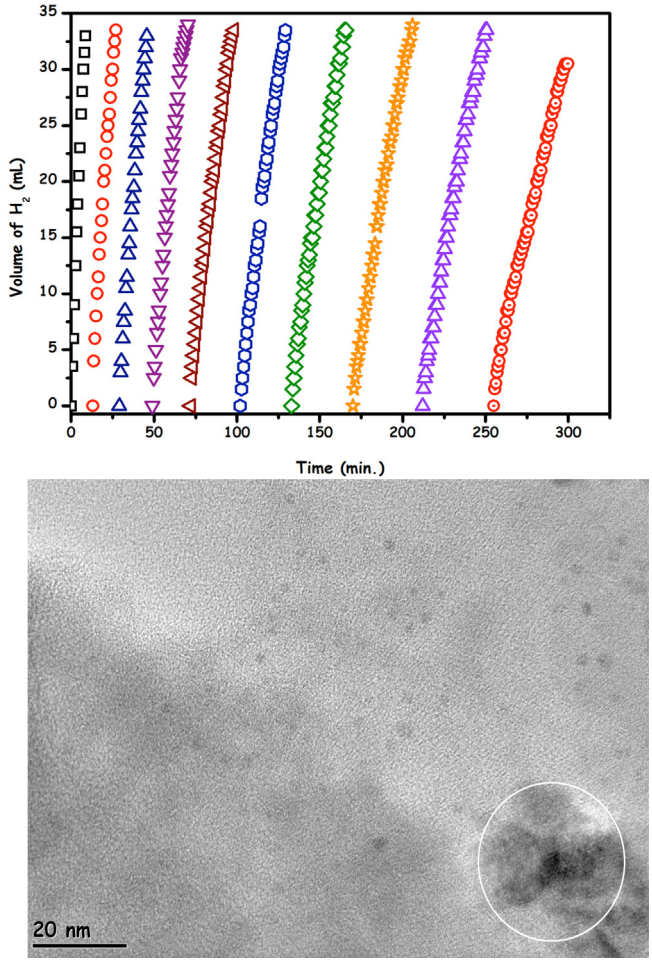

Fig. 10. Plot of volume of H_2 generated (mL) versus time (min.) up to 10 reuse for the the $Cu_{0.49}Co_{0.51}$/C catalyzed hydrolytic dehydrogenation of AB ([AB] = 100 mM, $M_{catalyst}$ in 1st run = 100 mg, $M_{catalyst}$ in 10th run = 50 mg in 5.0 mL H_2O) at 298 K and BFTEM image of $Cu_{0.49}Co_{0.51}$/C catalyst harvested after the 10th catalytic reuse; clumped CuCo NPs region was indicated by white circle.

constants k_{obs} determined from the nearly linear portions of the each plots at four different temperatures (Fig. 9(a)) are used to plot Arrhenius and Eyring plots (Fig. 9(b) and (c)) to calculate activation parameters: activation energy Ea = 51.9 kJ/mol, activation enthalpy $\Delta H^{\neq}$ = 48.5 kJ/mol and activation entropy $\Delta S^{\neq}$ = −89.9 J/mol K. Assuming that the apparent activation parameters calculated from the macroscopic kinetic data given above are relevant to the most critical activation step in the AB hydrolytic dehydrogenation mechanism, one can argue that the large positive magnitude of the apparent activation enthalpy and the large negative value of apparent activation entropy imply the presence of an associative mechanism at the transition state.

The catalytic stability of the $Cu_{0.49}Co_{0.51}$/C catalyst in the hydrolytic dehydrogenation of AB was investigated by performing reusability experiments. After the complete hydrolytic dehydrogenation of AB, $Cu_{0.49}Co_{0.51}$/C catalyst was isolated as a black powder and bottled under nitrogen atmosphere. Then, the isolated $Cu_{0.49}Co_{0.51}$/C catalyst was re-dispersed in the aqueous AB solution. This re-dispersed catalyst preserved 95% of its initial activity with a 90% conversion of AB to NH_4BO_2 and H_2 even at 10th catalytic reuse (Fig. 10). BFTEM image of $Cu_{0.49}Co_{0.51}$/C catalyst harvested after 10th catalytic reuse (Fig. 10) shows the existence of well-dispersed 1.9 nm CuCo NPs along with slightly clumped CuCo NPs consistent with the minor decrease (∼5%) observed in the activity of $Cu_{0.49}Co_{0.51}$/C catalyst at 10th catalytic reuse. Moreover, ICP-OES analyses of isolated $Cu_{0.49}Co_{0.51}$/C catalyst and reaction solution from 10th catalytic reuse gave us (*i*) almost the identical copper and cobalt amounts with those of the fresh catalyst and (*ii*) no leaching of metals into the reaction solution. Additionally, the hydrolytic dehydrogenation of AB can completely be stopped by removing $Cu_{0.49}Co_{0.51}$/C catalyst from the reaction solution. These results are indicative of the high stability of $Cu_{0.49}Co_{0.51}$/C catalyst against agglomeration and leaching throughout the catalytic runs.

4. Conclusions

In the current study, carbon supported CuCo NPs were prepared, characterized and used as heterogeneous catalyst in the hydrolytic dehydrogenation of AB. Some of the major findings of this study can be summarized as follows:

(a) CuCo/C was prepared, for the first time, by using a simple procedure with high reproducibility. The characterization of this new catalytic material by means of ICP-OES, PXRD, XPS, BFTEM, HRTEM, STEM, STEM-EDX and HAADF-STEM techniques revealed that the formation of well-dispersed 1.8 ± 0.4 nm CuCo alloy NPs on the surface of activated carbon.

(b) The catalytic employment of CuCo/C was demonstrated in the hydrolytic dehydrogenation of AB, which has been considered as one of the promising materials for the efficient chemical hydrogen storage. CuCo/C catalyst was found to be highly active catalyst in this reaction providing an initial turnover frequency of TOF = 2700 mol H_2 mol catalyst^{-1} h^{-1} at room temperature, which is not only higher than all the non-noble metal catalysts but also higher than the majority of the noble metal based homogeneous and heterogeneous catalysts employed in the same reaction.

(c) Testing the isolability and reusability of CuCo/C showed that CuCo/C catalyst isolated from the 9th catalytic reuse still acts as active catalyst in the 10th run of the hydrolytic dehydrogenation of AB > 95% of initial activity and conversion. ICP-OES and BFTEM analyses of the sample harvested from 10th catalytic reuse showed that CuCo alloy NPs show exceptional stability against to agglomeration and leaching throughout the catalytic reaction.

(d) The quantitative kinetic studies depending on catalyst [CuCo] and substrate [AB] concentrations reveal that CuCo/C catalyzed hydrolytic dehydrogenation of AB is half-order in catalyst concentration and zero order in substrate concentration. CuCo/C catalyzed hydrolytic dehydrogenation of AB was also investigated by performing this catalytic reaction at different temperatures to evaluate the activation parameters (Ea = 51.9 kJ/mol, $\Delta H^{\neq}$ = 48.5 kJ/mol and $\Delta S^{\neq}$ = −89.9 J/mol K). The activation enthalpy and activation entropy values are suggestive of the associative mechanism for CuCo/C catalyzed hydrolytic dehydrogenation of AB.

Understanding the existing synergistic effects in CuCo/C catalyst remains an active area of research in our group. More detailed experimental studies on the mechanism of CuCo/C catalyzed not only hydrolysis but also dehydrocoupling of AB are still underway. This uniquely active, selective and stable catalytic material has a strong potential to be exploited in practical/technological applications, where AB is utilized as a viable hydrogen carrier in mobile fuel cell applications.

Acknowledgments

The partial supports by Fevzi Akkaya Scientific Activities Support Fund (FABED), Science Academy and Turkish Academy of Sciences (TUBA) are gratefully acknowledged.

References

[1] J. Graetz, Chem. Soc. Rev. 38 (2009) 73–82.
[2] N.Z. Muradova, T.N. Veziroglu, Int. J. Hydr. Energy 30 (2005) 225–237.
[3] J.A. Turner, Science 285 (1999) 687–689.
[4] L. Schlaphach, A. Zuttel, Nature 414 (2001) 353–358.
[5] C. Berg, C. Arean, Chem. Commun. (2008) 668.
[6] W. Grochala, P.P. Edwards, Chem. Rev. 104 (2004) 1283.
[7] Q.L. Zhu, Q. Xu, Energy Environ. Sci. 8 (2015) 478.
[8] A. Staubitz, A. Robertson, I. Manners, Chem. Rev. 110 (2010) 4079.
[9] S. Satyapala, J. Petrovic, C. Read, G. Thomas, G. Ordaz, Catal. Today 120 (2007) 246.
[10] G. Wolf, J. Baumann, F. Baitalow, F.P. Hoffmann, Thermochim. Acta 343 (2000) 19.
[11] M. Yurderi, A. Bulut, I.E. Ertas, M. Zahmakiran, M. Kaya, App. Catal. B: Environ. 165 (2015) 169.
[12] C.A. Jaska, K. Temple, A.J. Lough, I. Manners, J. Am. Chem. Soc. 125 (2003) 9424.
[13] M. Zahmakiran, S. Özkar, Top. Catal. 56 (2013) 1171–1183.
[14] T. Umegaki, J.-M. Yan, X.-B. Zhang, H. Shioyama, N. Kuriyama, Q. Xu, Int J. Hydr. Energy 34 (2009) 2303.
[15] H.L. Jiang, S.K. Singh, J.M. Yan, X.B. Zhang, Q. Xu, ChemSusChem 3 (2010) 541.
[16] H.L. Jiang, Q. Xu, Catal. Today 170 (2011) 56.
[17] M. Zahmakiran, S. Ozkar, Nanoscale 3 (2011) 3462.
[18] M. Chandra, Q. Xu, J. Power Sources 156 (2006) 190.
[19] M. Chandra, Q. Xu, J. Power Sources 168 (2007) 135.
[20] M. Zahmakıran, S. Ozkar, App. Catal. B: Environ. 89 (2009) 104.
[21] M. Zahmakıran, F. Durap, S. Ozkar, Appl. Catal. A: Gen. 363 (2009) 53.
[22] H.L. Jang, T. Umegaki, T. Akita, X.B. Zhang, M. Horuta, Q. Xu, Chem. Eur. J. 16 (2010) 3132.
[23] J.M. Yan, X.B. Zhang, T. Akita, M. Horuta, Q. Xu, J. Am. Chem. Soc. 132 (2010) 5326.
[24] K. Aranishi, H.L. Jiang, T. Akita, M. Horuta, Q. Xu, Nano Res. 4 (2011) 1233.
[25] J.M. Yan, X.B. Zhang, S. Han, H. Shioyama, Q. Xu, Angew. Chem. Int. Ed. 47 (2008) 2287.
[26] Z.-H. Lu, J. Li, A. Zhu, Q. Yao, W. Huang, R. Zhou, R. Zhou, X. Chen, Int. J. Hydr. Energy 38 (2013) 5330.
[27] K. Mori, T. Taga, H. Yamashita, ChemCatChem 7 (2015) 1285.
[28] Q. Xu, M. Chandra, J. Power Sources 163 (2006) 364.
[29] Q. Xu, H. Shioyama, X.B. Zhang, J.M. Yan, J. Power Sources 195 (2010) 1091.
[30] O. Metin, S. Ozkar, Energy Fuels 23 (2009) 3517.
[31] B.R. Jagirdar, M. Indirani, S.B. Kalindi, Inorg. Chem. 47 (2008) 7424.
[32] Q. Xu, H. Shioyama, X.B. Zhang, J.M. Yan, J. Power Sources 195 (2010) 1091.
[33] M. Rakap, S. Ozkar, Int. J. Hydr. Energy 35 (2010) 3341.
[34] T. Umegaki, J.M. Yon, X.B. Zhang, H. Shioyama, Q. Xu, J. Power Sources 195 (2010) 8209.
[35] O. Metin, S. Ozkar, Int J. Hydr. Energy 36 (2011) 1424.
[36] O. Metin, M. Dinç, Z.S. Eren, S. Ozkar, Int J. Hydr. Energy 36 (2011) 11528.
[37] J. Li, Q.-L. Zhua, Q. Xu, Catal. Sci. Technol. 5 (2015) 525.
[38] T. Umegaki, J.M. Yon, X.B. Zhang, H. Shioyama, N. Kuriyama, Q. Xu, Int J. Hydr. Energy 34 (2009) 3816.
[39] T. Umegaki, J.M. Yon, X.B. Zhang, H. Shioyama, N. Kuriyama, Q. Xu, J. Power Sources 191 (2009) 209.
[40] J.M. Yon, X.B. Zhang, S. Han, H. Shioyama, Q. Xu, Inorg. Chem. 48 (2009) 7389.
[41] C.Y. Cao, C. Chen, W. Li, W.G. Song, W. Cai, ChemSusChem 3 (2010) 1241.
[42] M. Zahmakıran, T. Ayvalı, S. Akbayrak, S. Çalışkan, D. Celik, S. Ozkar, Catal. Today 170 (2011) 76.
[43] H.L. Jiang, T. Umegaki, T. Akita, X.-B. Zhang, M. Haruta, Q. Xu, Chem. Eur. J. 16 (2010) 3132.
[44] C. Xiang, J. Cheng, Z. She, Y. Zou, H. Chu, S. Qiu, H. Zhang, L. Sun, F, Xua RSC Adv. 5 (2015) 163.
[45] B.R. Jagirdar, U. Sanyal, B.B. Kalindirdi, Phys. Chem.Chem. Phys. 10 (2008) 5870.
[46] M. Zahmakıran, F. Durap, S. Ozkar, Int J. Hydr. Energy 35 (2010) 187.
[47] Y. Kamada, K. Yano, Q. Xu, S. Fukuzumi, J. Phys. Chem. C 114 (2010) 16456.
[48] M. Kaya, M. Zahmakiran, M. Volkan, S. Ozkar, ACS App. Mater. Int. 4 (2012) 3866.
[49] R.J. White, R. Luque, V.L. Budarin, J.H. Clarka, D.J. Macquarrie, Chem. Soc. Rev. 38 (2009) 481.
[50] Joint Committee on Powder Diffraction Standards, JCPDS International Center for Diffraction Data, Pennsylvania, (1991).
[51] N. Arul Dhas, C. Paul Raj, A. Gedanken, Chem. Mater. 10 (1998) 1446.
[52] M. Zahmakiran, S. Ozkar, T. Kodaira, T. Shiomi, Mater. Lett. 63 (2009) 400.
[53] M. Zahmakiran, S. Ozkar, Mater. Lett. 63 (2009) 1033.
[54] J.E. Hutchison, G.H. Woehrie, S. Özkar, R.G. Finke, Turk. J. Chem. 30 (2006) 1.
[55] V.F. Puntes, K. Krishnan, A.P. Alivisatos, Topics Catal. 19 (2002) 145.
[56] P.O. Gartland, S. Berge, B.J. Slagsvold, Phys. Rev. Lett. 28 (1972) 738.
[57] G.K. Hall, H.B. Mee, Phys. Sta. Sol. A 5 (1971) 389.
[58] A.K. Singh, Q. Xu, ChemCatChem 5 (2013) 652.
[59] F. Durap, M. Zahmakıran, S. Ozkar, Int. J. Hydr. Energy 34 (2009) 7223.
[60] T.J. Clark, R.G. Whittell, I. Manners, Inorg. Chem. 46 (2007) 7522.
[61] V.I. Simagina, P.A. Storozhenko, O.V. Netskina, O.V. Komova, G. Odegova, Y.V. Larichev, A.V. Ishchenko, A.M. Ozerova, Catal. Today 138 (2008) 253.
[62] M. Rakap, S. Ozkar, Int. J. Hydr. Energy 35 (2010) 1305.
[63] R. Ciganda, M.A. Garralda, L. Ibarlucea, E. Pinilla, M.R. Torres, Dalton Trans. 39 (2010) 7226.
[64] T.W. Graham, C.W. Tsang, X. Chen, R. Guo, W. Jia, S.M. Lu, C. Sui-Seng, C.B. Ewart, A. Lough, D. Amoroso, K. Abdur-Rashid, Angew. Chem. Int. Ed. 49 (2010) 8708.